Note on Earthquake Seismology <1> Quantitative Framework

Hideo Aochi

1. Quantitaive Framework
2. Crack theory and fracture
3. Earthquake scaling
4. Friction
5. Numerical model
6. Obsevational seismology

Mechanical point of view

1. Equation of motion of the medium $\rho\ddot{u} = \nabla \cdot \tau$

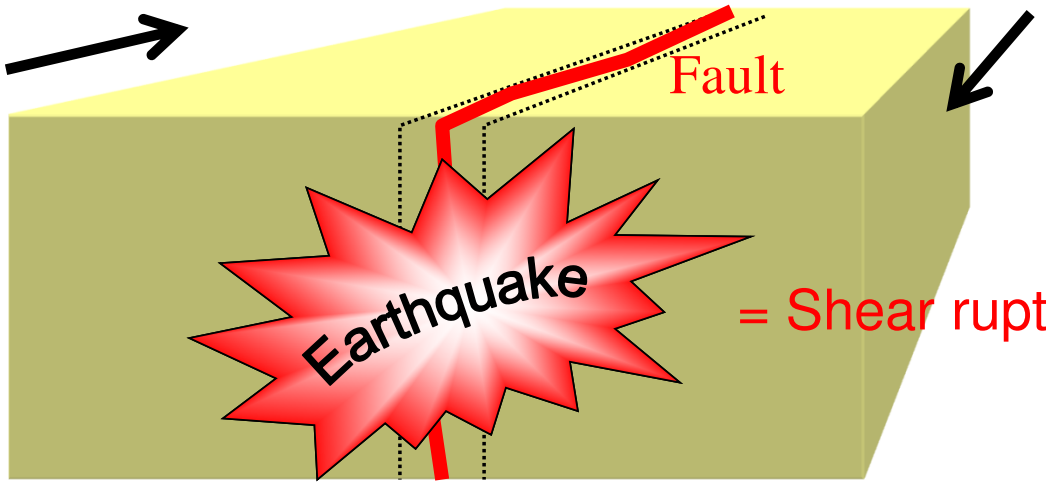

= Shear rupture

3. Initial Condition (Loading)

$\tau = \tau_0$

2. Boundary condition (Friction) $\tau = \tau(\Delta u, \Delta \dot{u}, t, T, \cdots)$

Field earthquake (M7)	**30 km**	**>1 m**	**~10 MPa**	**m/s**	**km/s**
	Dimension	***Slip***	***Stress***	***Slip rate***	***Rupture velocity***
Laboratory	**<10 cm**	**<mm**	**1-100MPa**	**m/s**	**km/s**

Seismological point of view

Earthquake is a phenomenon that strain energy accumulated in the Earth's interior is suddenly released.

Eshelby (1957)

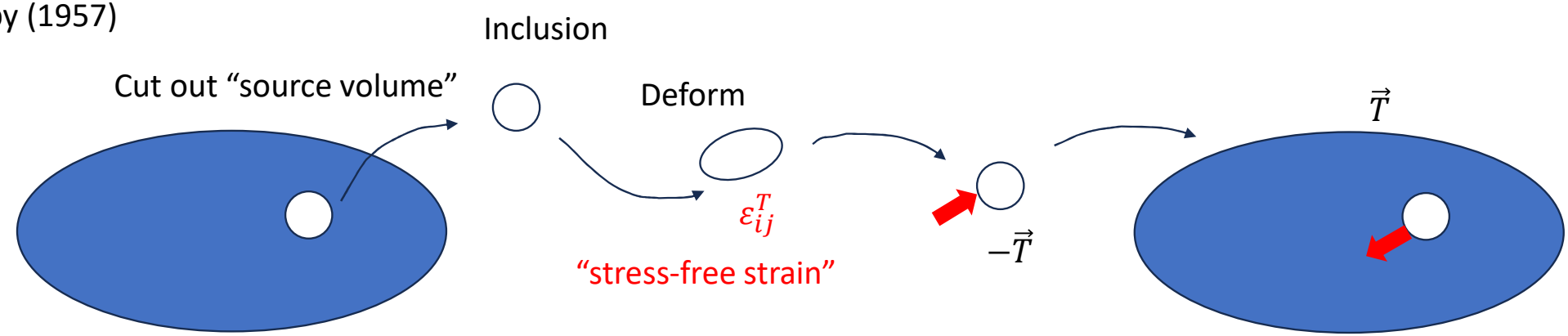

$$u_i(x,t) = \iint_S T_k(x',t) * G_i^k(x-x',t)dS = \iint_S \sigma_{kj}^T(x',t)n_j * G_i^k(x-x',t)dS$$

Linear response of elastic medium

Green's function

Moment tensor: $$M_{ij}(t) = \iiint_V \sigma_{ij}^T(t)dV$$

Green function

Medium response due to an impulsive point force

3D isotropic, infinite, homogeneous elastic medium

$$G_i^k(x,t) = \frac{1}{4\pi\rho r^3}(3\gamma_i\gamma_k - \delta_{ik})\int_{\frac{r}{\alpha}}^{\frac{r}{\beta}} \tau\delta(t-\tau)d\tau + \frac{1}{4\pi\rho\alpha^2 r}\gamma_i\gamma_k\delta\left(t-\frac{r}{\alpha}\right) + \frac{1}{4\pi\rho\beta^2 r}(\delta_{ik} - \gamma_i\,\gamma_k)\delta\left(t-\frac{r}{\beta}\right)$$

$$\gamma_i = \frac{x_i - x'_i}{r}$$

2D SH case (anti-plane)

$$G_{33}(x,t) = \frac{1}{2\pi\mu}\frac{H(t-\frac{r}{\beta})}{\sqrt{t^2 - r^2/\beta^2}}$$

2D P-SV case (in-plane)

$$G_{11} = \frac{1}{2\pi\rho}\frac{\partial^2}{\partial x_1^2}\left(I_\alpha - I_\beta\right) + G_{33}$$

$$G_{22} = \frac{1}{2\pi\rho}\frac{\partial^2}{\partial x_{21}^2}\left(I_\alpha - I_\beta\right) + G_{33}$$

$$G_{12} = \frac{1}{2\pi\rho}\frac{\partial^2}{\partial x_1 \partial x_2}\left(I_\alpha - I_\beta\right)$$

$$I_c \equiv \left\{ t\log\left[\frac{ct}{r} + \sqrt{\left(\frac{ct}{r}\right)^2 - 1} - \sqrt{t^2 - \left(\frac{r}{c}\right)^2}\right]\right\} H\left(t-\frac{r}{c}\right); c = \alpha, \beta$$

Displacement field due to moment tensor

$$u_i\ (x,t) = \frac{1}{4\pi\rho}\left[\frac{15\gamma_i\gamma_j\gamma_k - 3\gamma_i\delta_{jk} - 3\gamma_j\delta_{ki} - 3\gamma_k\delta_{ij}}{r^4}\int_{\frac{r}{\alpha}}^{\frac{r}{\beta}} \tau M_{jk}(t-\tau)d\tau\right.$$
$$+\frac{6\gamma_i\gamma_j\gamma_k - \gamma_i\delta_{jk} - \gamma_j\delta_{ki} - \gamma_k\delta_{ij}}{\alpha^2 r^2}\ M_{jk}\left(t-\frac{r}{\alpha}\right)$$
$$-\frac{6\gamma_i\gamma_j\gamma_k - \gamma_i\delta_{jk} - \gamma_j\delta_{ki} - 2\gamma_k\delta_{ij}}{\beta^2 r^2}\ M_{jk}\left(t-\frac{r}{\beta}\right)$$
$$\left.+\frac{\gamma_i\gamma_j\gamma_k}{\alpha^3 r}\ \dot{M}_{jk}\left(t-\frac{r}{\alpha}\right)+\frac{\delta_{ij}\gamma_k - \gamma_i\gamma_j\gamma_k}{\beta^3 r}\ \dot{M}_{jk}\left(t-\frac{r}{\beta}\right)\right]$$

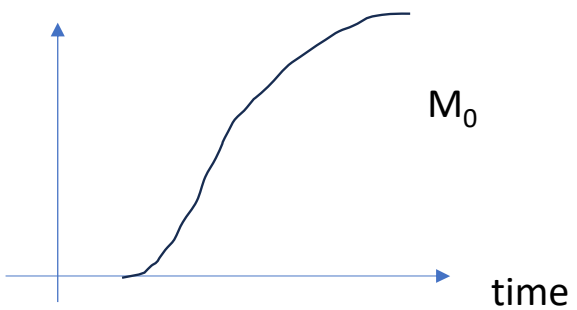

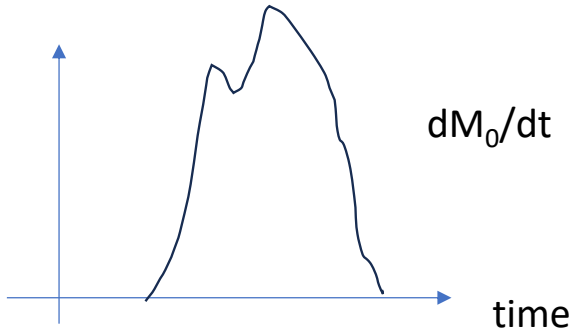

Representation theorem

$$u_i(x,t) = \int_{-\infty}^{t} d\tau \int_S \left[G_i^p(x,t;\xi,\tau) T_p(\xi,\tau) - u_k(\xi,\tau) H_i^k(x,t;\xi,\tau) \right] dS$$

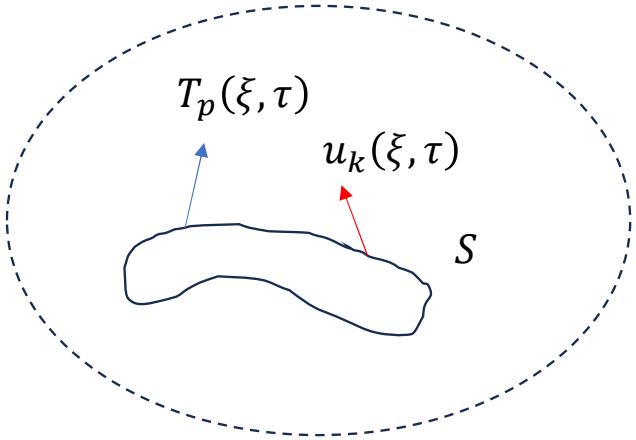

Faulting (no width) $\quad \Delta u \equiv u^+(\xi,\tau) - u^-(\xi,\tau)$

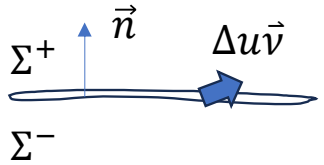

$$u_i(x,t) = \int_{-\infty}^{t} d\tau \int_\Sigma \Delta u_k(\xi,\tau) c_{klpq}(\xi) n_l(\xi) \frac{\partial}{\partial \xi_q} G_{ip}(x,t;\xi,\tau)\, dS$$

Moment tensor density corresponding faulting $\quad m_{pq}(\xi,t) = \mu \Delta u(\xi,t)(n_p \nu_q + n_q \nu_p)$

Far-field displacement $\quad u_i(x,t) \sim C_i \frac{\mu}{4\pi\rho c^3 R} \int_\Sigma \Delta \dot{u}(\xi, t - R/c)\, dS \qquad c = V_P$ and V_S

In Fourier domain $\Rightarrow \quad u_i(x,\omega) = S(\omega) \cdot P(x,\omega)$

Kinematic source description:

U=uniform, Vr=const

Haskel's model (1964)
Kostrov (1964)-Sato and Hirasawa (1973)
Madariaga (1976)

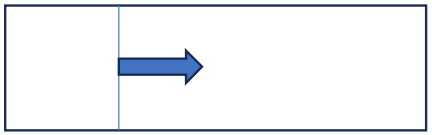

Unilateral rupture

Self-similar model

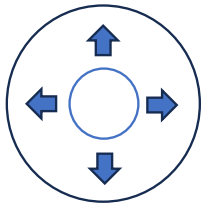

Circular dislocation

$$\Delta u(r,t) = \frac{24}{7\pi}\frac{\Delta\sigma}{\mu}\sqrt{{V_r}^2 t^2 - r^2}\cdot H\left(t - \frac{r}{v_r}\right);\ v_r t \le a$$

Far-field displacement

$$\Omega(r,t) = \frac{24}{7\pi}\frac{\Delta\sigma}{\mu}\frac{2\pi {v_r}^3}{\left[1-\left(\frac{v_r}{c}\right)^2 sin^2\theta\right]^2}\left(t-\frac{R}{c}\right)^2;\ R/c_r \le t \le Rc + a/v_r$$

Seismic energy

Seismic energy flow out of the elastic body (dissipitaiton)

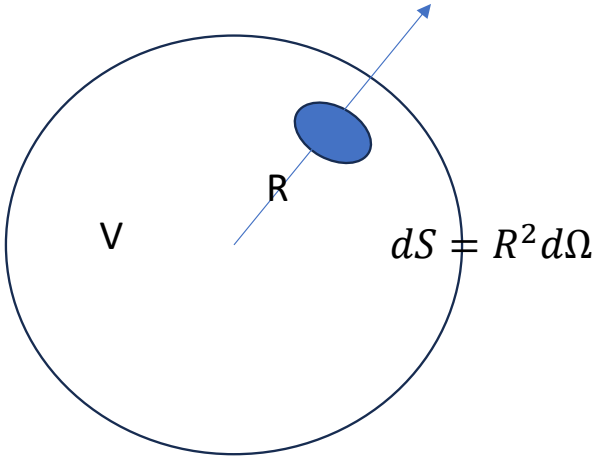

$$E_s = -\int_0^t d\tau \int_S \sigma_{ij}\dot{u}_i n_j dS = -K(t) - \Delta U(t) + \int_0^t dt \int_V f_i \dot{u}_i dV$$

Kinetic energy

Work of the sources

Strain energy

$$\dot{e}_s d\Omega = \sigma_{ij}\dot{u}_i n_j R^2 d\Omega = \rho c \dot{u}_i^2 R^2 d\Omega \qquad \sigma_{ij} n_j \cong \rho c \dot{u}_i \quad \text{(far field)}$$

From velocity waveforms

$$e_c = \rho c R^2 \int_0^\infty \dot{u}_i^2(\tau) d\tau$$

From source time function

$$e_c = \frac{1}{16\pi^2 \rho c^5} \langle R^c \rangle_2 \int_0^\infty \dot{s}^2(\tau) d\tau$$

$$E_s = \frac{1}{16\pi} \langle R^c \rangle_2 \frac{M_0^2 \omega_0^3}{\rho c^5}$$

Bulletin of the
Seismological Society of America

Vol. 66 June 1976 No. 3

DYNAMICS OF AN EXPANDING CIRCULAR FAULT

BY RAUL MADARIAGA

ABSTRACT

We study a plane circular model of a frictional fault using numerical methods. The model is dynamic since we specify the effective stress at the fault. In one model we assume that the fault appears instantaneously in the medium; in another, that the rupture nucleates at the center and that rupture proceeds at constant subsonic velocity until it suddenly stops. The total source slip is larger at the center and the rise time is also longer at the center of the fault. The dynamic slip overshoots the static slip by 15 to 35 per cent. As a consequence, the stress drop is larger than the effective stress and the apparent stress is less than one half the effective stress.

The far-field radiation is discussed in detail. We distinguish three spectral regions. First, the usual constant low-frequency level. Second, an intermediate region controlled by the fault size and, finally, the high-frequency asymptote. The central region includes the corner frequency and is quite complicated. The corner frequency is shown to be inversely proportional to the width of the far-field displacement pulse which, in turn, is related to the time lag between the stopping phases. The average corner frequency of S waves v_0^s is related to the final source radius, a, by $v_0^s = 0.21\,\beta/a$. The corner frequency of P waves is larger than v_0^s by an average factor of 1.5.

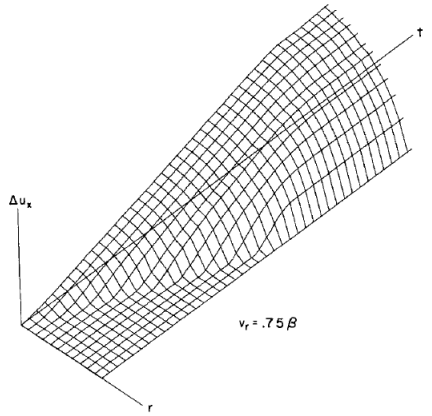

FIG. 3. Source slip function for a subsonic circular fault with $v_R = 0.75\beta$. This is a composite plot of the slip history as a function of radius on the fault.

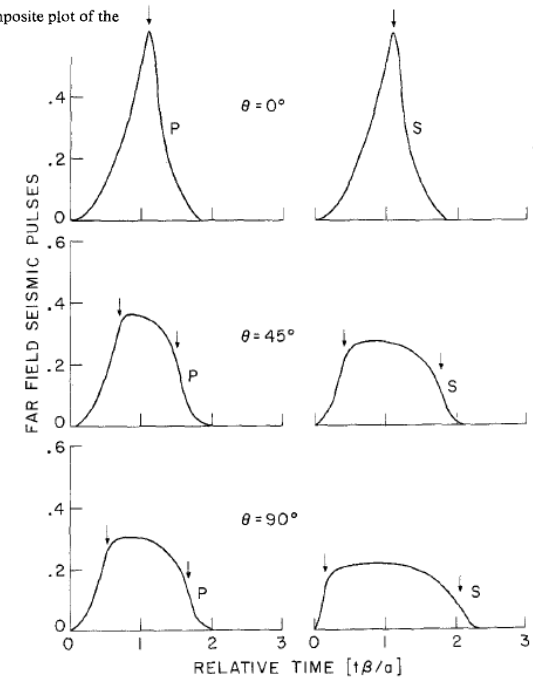

FIG. 9. Far-field displacement pulses radiated by a subsonic circular fault. Time is measured relative to the arrival from the nucleation point at the center of the fault. The arrows indicate the arrival time of stopping phases from the nearest and farthest points on the edge of the fault. The displacement pulses are scaled by a constant time integral (constant low-frequency level).

$$M_0 = \mu\bar{u}\pi a^2 = \frac{16}{7}\Delta\sigma a^3$$ (Keilis-Book, 1959)

ELSEVIER

Tectonophysics 261 (1996) 209–227

TECTONOPHYSICS

Properties of the seismic nucleation phase

Gregory C. Beroza [a,*], William L. Ellsworth [b]

[a] *Department of Geophysics, Stanford University Stanford, CA 94305-2215, USA*
[b] *US Geological Survey Menlo Park, CA 94025, USA*

Received 25 August 1995; accepted 15 November 1995

Abstract

Near-source observations show that earthquakes begin abruptly at the P-wave arrival, but that this beginning is weak, with a low moment rate relative to the rest of the main shock. We term this initial phase of low moment rate the seismic nucleation phase. We have observed the seismic nucleation phase for a set of 48 earthquakes ranging in magnitude from 1.1–8.1. The size and duration of the seismic nucleation phase scale with the total seismic moment of the earthquake, suggesting that the process responsible for the seismic nucleation phase carries information about the eventual size of the earthquake. The seismic nucleation phase is characteristically followed by quadratic growth in the moment rate, consistent with self-similar rupture at constant stress drop. In this paper we quantify the properties of the seismic nucleation phase and offer several possible explanations for it.

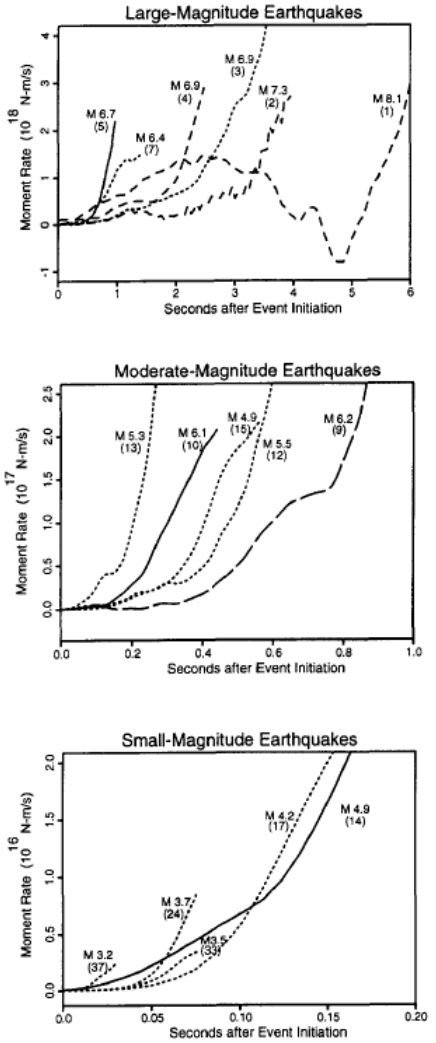

Fig. 3. Moment-rate functions for the initiation of small, medium, and large earthquakes determined by deconvolution. Numbers in parentheses refer to the numbers used in Table 1. Each earthquake begins weakly then abruptly accelerates. Each panel is plotted at a different time scale. The time between initiation ($t = 0$ on the plot) and the initiation of high moment rate varies systematically with earthquake size.

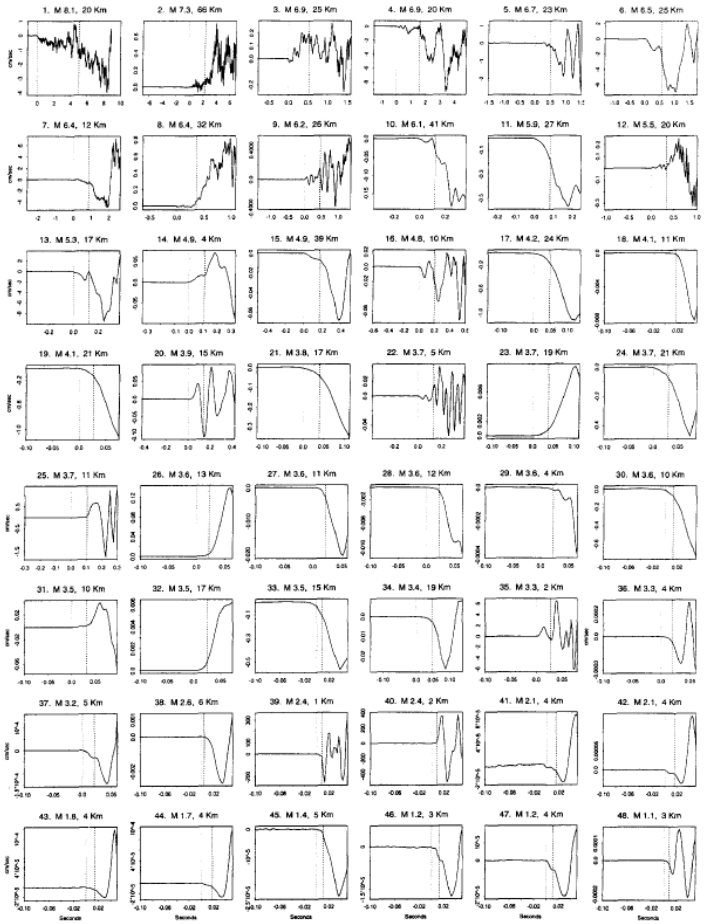

Fig. 7. The seismic nucleation phase for the 48 earthquakes that we studied shown using velocity seismograms (cm/s). Zero time on the plot and the first dashed line indicates the arrival time of the first seismic wave. The interval between that and the second dashed vertical line spans the duration, ν, of the nucleation phase. Self-similar growth of a constant stress drop crack predicts a linear increase in velocity with time, which we typically don't observe until the end of the seismic nucleation phase. We term the linear growth that starts at the end of ν the breakaway phase.

JGR Solid Earth

RESEARCH ARTICLE
10.1029/2019JB018045

How Does Seismic Rupture Accelerate? Observational Insights From Earthquake Source Time Functions

Julien Renou[1], **Martin Vallée**[1], **and Pierre Dublanchet**[2]

[1]Université de Paris, Institut de physique du globe de Paris, CNRS, Paris, France, [2]MINES ParisTech, PSL Research University, Centre de Géosciences, Fontainebleau, France

Key Points:
- Source time functions exhibit a magnitude-independent signal during periods of monotonically increasing moment rate
- Moment rate time evolution in the development phase does not follow the steady quadratic self-similar growth
- Rupture models with variable rupture velocity and/or stress drop are required to reproduce the observations

Supporting Information:
- Supporting Information S1

Correspondence to:
J. Renou,
renou@ipgp.fr

Citation:
Renou, J., Vallée, M., & Dublanchet, P. (2019). How does seismic rupture accelerate? Observational insights from earthquake source time functions. *Journal Geophysical*

Abstract Observation of the seismic process for a large earthquake population is of key interest to detect potential magnitude-dependent behaviors and, more generally, to quantify how seismic rupture develops. In contrast with studies focusing on the first radiated waves, we here propose to characterize the growing phase leading to the main seismic moment release episode(s), which we refer to as the development phase. Our analysis uses the 2,221 teleseismic source time functions (STFs) of shallow dip-slip earthquakes provided by the global SCARDEC database and consists in measuring the moment acceleration during the development phase at prescribed moment rates. This approach is therefore insensitive to hypocentral time uncertainties and aims at quantifying how seismic ruptures accelerate, independently of when they accelerate. Our results first show that rupture acceleration does not exhibit any magnitude-dependent signal emerging above the intrinsic measurements variability. We thus use the full STF catalog to characterize the moment rate $\dot{M}_d$ of the development phase and show that, on average, $\dot{M}_d(t) \propto t^{n_d}$ with n_d equal to 2.7. This time evolution therefore does not follow the steady t^2 growth expected for classical circular crack models, which indicates that stress drop and/or rupture velocity transiently vary during the development phase. We finally illustrate with a synthetic STF catalog that, due to initial rupture variability, approaches based on hypocentral time are not expected to fully characterize the behavior of the development phase.

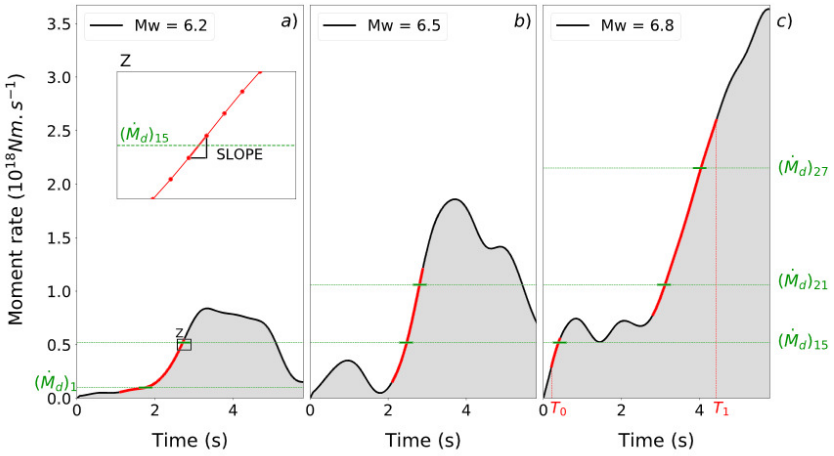

Figure 1. Examples of extraction of the development phase (in red) for representative STF shapes. In (a) and (b), STFs have a monotonic section connecting the values between $0.07F_m$ and $0.7F_m$. Panel (c) is an example of STF with complex shape in which development phase is extracted in the $[T_0 T_1]$ time interval (see section 2.1). These three illustrative events have different magnitudes and their development phases start at different times. Moment acceleration is computed at the time where the development phase crosses the prescribed moment rates $(\dot{M}_d)_i$, if this intersection exists. Four examples of $(\dot{M}_d)_i$ values (for $i = 1, 15, 21$, and 27) are shown in green. The sampling rate is equal to 0.07 s. Note that the approximate reference time shown in the bottom of each STF is not used in this approach.

Further reading

- Brune (1970). https://doi.org/10.1029/JB075i026p04997

- Madariaga, R. (2011). Earthquake Scaling Laws. In: Meyers, R. (eds) Extreme Environmental Events. Springer, New York, NY. https://doi.org/10.1007/978-1-4419-7695-6_22